Additive Manufacturing 51 (2022) 102585

Contents lists available at ScienceDirect

Additive Manufacturing

journal homepage: www.elsevier.com/locate/addma

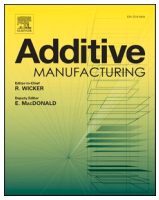

Effect of contaminations on the acoustic emissions during wire and arc additive manufacturing of 316L stainless steel☆

André Ramalho [a], Telmo G. Santos [a], Ben Bevans [b], Ziyad Smoqi [b], Prahalad Rao [b], J. P. Oliveira [a,*]

[a] UNIDEMI, Department of Mechanical and Industrial Engineering, NOVA School of Science and Technology, NOVA University Lisbon, 2829-516 Caparica, Portugal
[b] Department of Mechanical and Materials Engineering, University of Nebraska-Lincoln, Nebraska Hall, Lincoln, NE 68588, United States

ARTICLE INFO

Keywords:
Wire and arc additive manufacturing
Contamination
Acoustic spectrum
Additive manufacturing
Fast Fourier Transform

ABSTRACT

Additive Manufacturing (AM) processes allow the creation of complex parts with near net shapes. Wire and arc additive manufacturing (WAAM) is an AM process that can produce large metallic components with low material waste and high production rates. Typically, WAAM enables over 10-times the volumetric deposition rates of powder-based AM processes. However, the high depositions rates of WAAM require high heat input to melt the large volume of material, which in turn results in potential flaws such as pores, cracks, distortion, loss of mechanical properties and low dimensional accuracy. Hence, for practical implementation of the WAAM process in an industrial environment it is necessary to ensure flaw-free production. Accordingly, to guarantee the production-level scalability of WAAM it is fundamental to monitor and detect flaw formation during the process. The objective of this work is to characterize the effects of different contaminations on the acoustic spectrum of WAAM and lay the foundations for a microphone-based acoustic sensing approach for monitoring the quality of WAAM-fabricated parts. To realize this objective, WAAM parts were processed with deliberately introduced flaws, such as material contamination, and the acoustic signals were analyzed using the time and frequency domain techniques, namely, Power Spectral Density, and Short Time Fourier Transform. The signatures obtained were used to pinpoint the location of flaw formation. The results obtained in this study show that the effects of contamination in WAAM can be identified through the analysis of the acoustic spectrum of the process.

1. Introduction

Additive manufacturing (AM) processes have the potential to revolutionize design and manufacturing barriers due to their ability to build complex parts with near-net shape. Compared to traditional subtractive and formative manufacturing technologies, AM processes enable multiple key features including as mass customization, one-piece-flow, elimination of complex assemblies, reduced production time and material waste.

Two types of AM processes have emerged as the choice for the production of metal components that use powder-based feedstock material, and these are: powder bed fusion (PBF) and direct energy deposition (DED) [1]. For example, in PBF systems thin layers of metal powder are spread (raked or rolled) on the build platform and selectively melted using an energy beam (a laser or an electron beam). Likewise, in powder DED processes the feedstock material is sprayed from nozzles onto a substrate and melted, typically, using a laser. Although the powder DED- and PBF-based AM processes allow the manufacturing of complex parts with high dimensional accuracy, they present low deposition rates [2]. Moreover, the powder material is relatively expensive, with the price per kilogram of stainless steel powder ranging between 30 and 80$ for example, depending on the powder quality and production method. While large volume parts can be created (some commercial DED machines have a build volume larger than one cubic meter [3]), the size of parts created with PBF with a typical production-scale machine are within 25 cm × 25 cm × 50 cm [4].

An alternative approach to overcome the low production rates and high cost of PBF and powder DED metal AM is the wire and arc additive

☆ One of the authors of this article is part of the Editorial Board of the journal. To avoid potential conflicts of interest, the responsibility for the editorial and peer-review process of this article lies with the journal's other editors. Furthermore, the authors of this article were removed from the peer review process and had no, and will not have any access to confidential information related to the editorial process of this article.

* Corresponding author.
E-mail address: jp.oliveira@fct.unl.pt (J.P. Oliveira).

https://doi.org/10.1016/j.addma.2021.102585
Received 17 September 2021; Received in revised form 23 December 2021; Accepted 27 December 2021
Available online 30 December 2021

manufacturing (WAAM) process, which is also a DED process. The WAAM process uses an electric arc as a heat source and a metallic wire as the feedstock material [5]. This process combines the concepts of conventional fusion welding processes [6] with an automated system to control the torch path and process parameters [7]. WAAM trades the dimensional accuracy and surface finish of PBF and powder DED for high deposition rates and ability to produce large parts, the lower cost of raw materials (stainless steel welding wire costs ~$10 per kg), reduced material waste and high deposition rates (up to 5 kg per hour) that lead to a high production rates [8].

For example, Martina et al. [9], studied the cost of producing titanium parts with WAAM in comparison to subtractive processes and verified that cost savings up to 70% can be achieved. Depending on the process parameters, i.e. welding current, voltage or travel speed, the microstructure and the material properties and forming accuracy can be drastically modified for different materials, as evidenced for steels [10,11], or stainless steels [12]. Several WAAM variants have also been developed to improve the process capabilities, such as the Hot Forging WAAM [13], Ultracold-WAAM [14], in-situ strengthening using high temperature particles [15] or ultrasonic vibration [16].

Despite its ability to create large parts in a cost-effective manner, WAAM has certain limitations that hinder its industrial application when compared to other AM processes, such as poor surface quality, distortion, variation in mechanical properties, and geometric accuracy. The non-uniform temperature distribution and the comparatively high input in WAAM is the root cause of flaw formation during the process. Considering the limitations mentioned before, the quality of the parts produced must be assured. However, the use of Non-Destructive Testing (NDT) in WAAM is a very demanding task, both in-line or off-line situations, due to the high surface irregularity, high temperature of the surface parts and the small dimensions of the generated defects [17,18]. In some situations the ability to inspect the parts post-production is also decreased due to the geometric complexity which does not allow the inspection of critical areas [5]. Accordingly, and to avoid the loss of the total part on advanced stages of production, there is a need for an online monitoring system to detect and identify flaw formation in WAAM parts during the process, as the part is being printed. The implementation of monitoring systems can also improve productivity and reliability while reducing production costs [19,20].

The fundamental phenomena in WAAM are similar to arc-based welding. In traditional arc welding processes, manual welders rely on visual and acoustic information to monitor the quality of the weld. In fact, experienced welders can spot welding defects just by hearing the sound during the process. Monitoring systems replicate the welder's judgment by using sensors to collect information about the weld pool and electric arc. Defects in WAAM can be attributed to several factors such as deficient parameter setup, poor deposition strategy, machine malfunction, or contamination [21]. The presence or introduction of contaminant materials during the printing of layers may disrupt the deposition process and ultimately lead to weld discontinuities and/or defects. These discontinuities lead to the variations of parameters that can be measured while the part is being produced. Since different types of sensors can capture various aspects of the process, the right choice of sensing and monitoring (diagnostic) system is of utmost importance.

The objective of this work is to characterize the effects of contaminations on the acoustic spectrum of WAAM and lay the foundations for a microphone-based acoustic sensing approach for monitoring the quality of WAAM-processed parts. Although some studies have been published regarding the use of acoustic sensors to identify the metal transfer mode [22], estimate the arc length [23] and assess the quality of arc welding processes [24], there are still few publications regarding WAAM acoustic data analysis, its correlation with process parameters and the identification of defects during part production. One of the pioneer studies in this field was conducted by Horvat et al. [25] which showed that from the sound emitted by the welding process, it is possible to identify the ignition and extinction of the electric arc and associate this with current and voltage data. Our work lays the foundations for the development of an acoustic monitoring system for WAAM and demonstrates the ability to identify and characterize defects generated during production of parts through this method thus opening new potential venues for adoption of acoustic sensing technology by the industry.

2. Experimental setup

2.1. Materials

The experimental setup consisted of a customized welding torch assembled on a three-axis positioning system [13]. The welding torch was connected to a welding machine *Kempi Pro MIG 3200* with a *Kempi Pro MIG 501* control unit. The feedstock material used was a commercial stainless steel 316L wire with 1 mm in diameter. The chemical composition of the wire feedstock material is detailed in Table 1.

2.2. Samples and processing

Thin-wall parts were deposited consisting of a single hatch (pass or bead per layer). Each part is comprised of 11 layers. Each layer had a thickness of 1.2 mm and a length of 120 mm and was deposited using a zig-zag deposition strategy. To maintain the heat transfer conditions similar for all the samples produced, the 316L stainless steel walls were built onto carbon steel substrates with dimensions of 200 × 60 × 10 mm. The wire feed speed was fixed at 4 m/min, the torch speed was set at 360 mm/min, the contact-tip-to-work distance was 8 mm, while the dwell time between deposited layers was 2 min. Argon (99.999%) was used as the shielding gas at a flow rate of 15 L/min. The process parameters used to produce the stainless steel parts were determined in such a way that no major process defects (cracks and/or pores, for example) were expected. These process parameters are detailed in Table 2.

To evaluate the effect of flaw formation on the acoustic signal during WAAM, flaws were embedded at predefined heights. Accordingly, two 2.5 mm diameter holes were drilled on layers #6 and #10, as schematically depicted in Fig. 1. These holes were then filled with foreign materials to simulate contamination during processing. These foreign materials include chalk, oil, and sand. WAAM, unlike powder bed fusion processes, occurs in open environments. For this, contamination of the part being produced can be fairly common as it occurs during conventional fusion welding. In fact, oil is one of the most typical contaminations during fusion-based arc processes, while other particles, mainly dust, can be picked up by the melt pool during production. For this reason, we have chosen to evaluate the impact of different contaminants, namely oil, chalk and sand on the acoustic emission of the WAAM process. All these contaminants can have different impacts on the process stability and defect formation. Chalk contaminations are not expected to occur during WAAM but this material was used to cause an exaggerated disturbance on the electric arc.

The intention of adding these different contaminants was to promote the disruption of the electric arc in a controlled manner. Being poor electrical conductors, chalk and sand were expected to change the frequency of formation of the electric arc, making the process more unstable. Oil was expected to generate porosity in the part while having a more subtle effect on the electric arc stability when compared to the other two contaminants, i.e., arc generation would be less affected. The effect that each of these contaminants will have on the arc disruption and subsequent defect formation during the WAAM process will be further discussed in Section 3.

Table 1
Chemical composition of stainless steel 316L, in wt%.

C	Mn	Si	P	S	Cr	Mo	Ni	N
0.03	1.80	0.75	0.045	0.03	18.50	2.6	12.5	0.1

Table 2
Process parameters used for WAAM of the 316L stainless steel parts.

Number of layers	11
Layer length [mm]	120
Torch speed [mm/min]	360
Wire feed speed [m/min]	4
Dwell time [s]	120
Gas flow rate [L/min]	15

The distance between the two holes within the same layer was of 40 mm to assess the duration and impact of the arc disruption as an effect of contaminant material. The schematic of the WAAM wall with the drilled holes is depicted in Fig. 1.

Table 3 details the sample identification used throughout the paper to identify each of the produced 316L stainless steel WAAM parts according to the contaminant used to disrupt the electric arc.

2.3. Process instrumentation

To acquire the acoustic signal during the WAAM process, a microphone was connected to the welding torch through a rigid support that allowed a constant distance of 250 mm between the microphone and the electric arc. The angle between the microphone and the substrate surface was set at 20º. Fig. 2 depicts the position of the microphone relatively to the welding torch.

The microphone used was a Shure SM57 dynamic microphone, with a cardioid polar pattern and a frequency response in the range of 40 Hz to 15 kHz. To record the acoustic signal, a National Instruments 9234 data acquisition card was used. Considering the frequency range limitations of the microphone and, according to the Nyquist-Shannon sampling theorem [26], the sampling rate used to acquire the acoustic signal was fixed at 25.6 kHz.

Apart from measuring the acoustic signal during the WAAM process, the electric voltage, and the electric current intensity of the arc were also acquired. With these measurements it is possible to identify, with precision, the time range in which the changes on the welding signal occur. The electric voltage was measured near the arc, between the tip of the torch and the substrate of the part, while the electric current was measured with a Hall effect current transducer (LEM HTA 600S). Both voltage and electrical current were recorded with a sampling rate of 3 kHz through a National Instruments 6008 data acquisition card. Fig. 3 details a schematic representation of the experimental setup.

Being a fully automated process, WAAM requires the use of several devices that guarantee its correct functioning. Each of these devices

Table 3
Sample identification according to the contaminant material.

Contaminant material	Sample ID
Chalk	C1
Oil	O1
Sand	S1

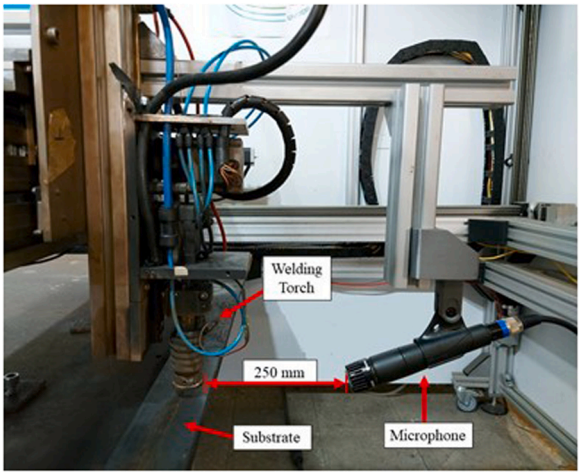

Fig. 2. Microphone placement relatively to the welding torch.

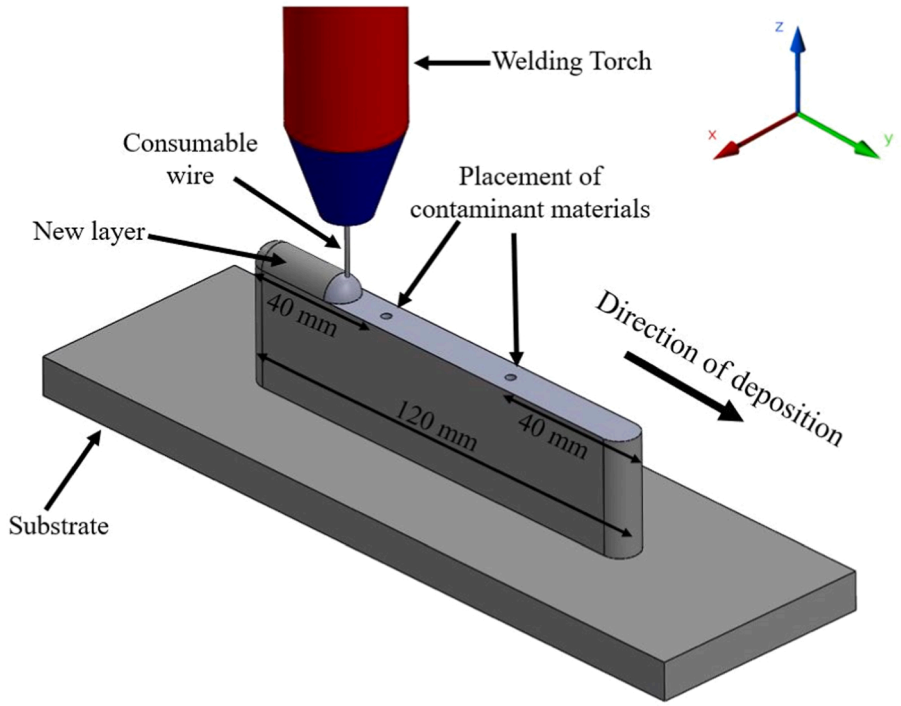

Fig. 1. Schematic representation of the placement of the contaminant materials and layer deposition process (Y is the deposition direction).

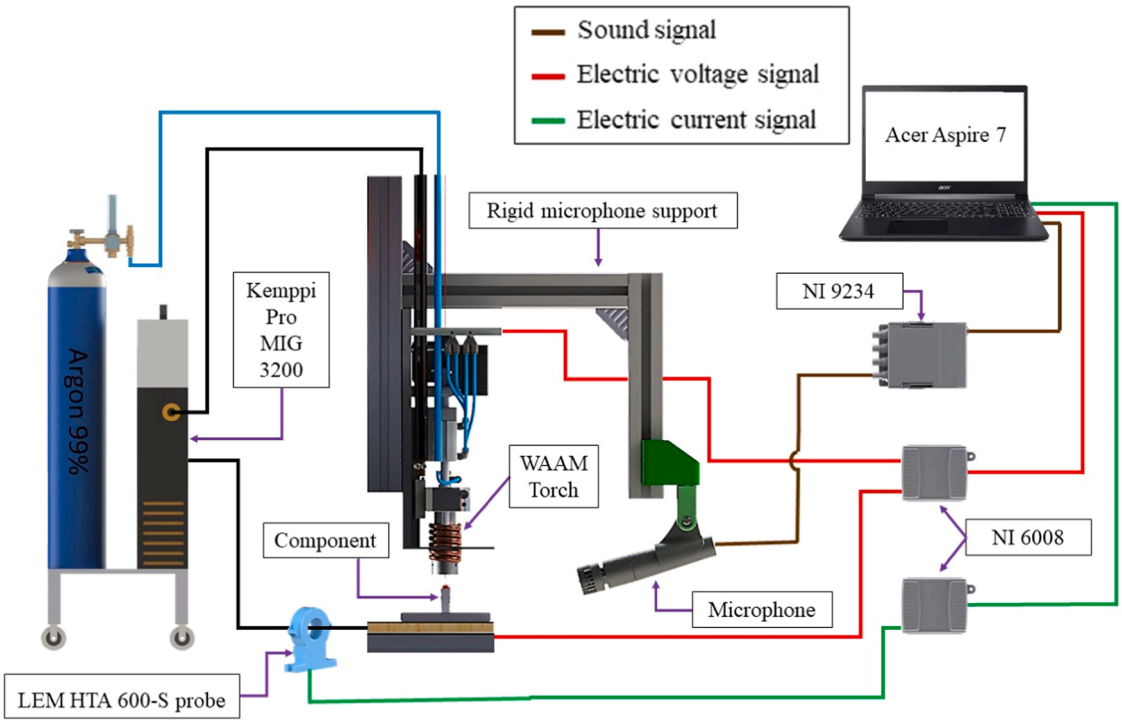

Fig. 3. Schematic representation of the experimental setup.

have their own acoustic signal that could interfere with the sound spectrum generated by the WAAM process and subsequently with the identification of potential defects. Considering this possible interference on the acoustic data, the following sound signals were isolated and analyzed for the selected operating conditions:

- Y axis bipolar step motor for a torch speed of 360 mm/min on;
- Shielding gas open;
- Fume extraction system on;
- Wire extruder with a wire feed speed of 4 m/min on;

Stratifying and isolating the acoustic signal from each of these machine elements is the critical first-step to eliminate ambient noise from the sensor data for effective characterization of the acoustic spectrum of the WAAM process, thus avoiding false alarm and failing-to-detect errors (Type I and type II errors, respectively).

After WAAM, the samples were analyzed using X-ray Computed Tomography (XCT) with a Nikon XTH255 ST system. The porosity analysis was performed at a resolution of 17 μm per voxel using the native Volume Graphics software.

2.4. Data processing

To identify potential arc perturbations or disruptions induced by the introduction of contaminant materials during WAAM, it is necessary to couple responsive sensing with signal analysis techniques that can capture evanescent phenomena from the recorded data. Accordingly, the acoustic data acquired during the WAAM process were examined using time domain, frequency domain and time-frequency domain signal analysis. The electric current and voltage data were only analyzed in the time domain to identify with precision the contamination intervals.

Time domain representation of the acoustic data captured through the microphone depicts the sound pressure as a function of time. The frequency distribution for each data set was analyzed by calculating the Power Spectral Density (PSD). Time-frequency domain analysis was performed using Short Time Fourier Transform (STFT). This type of data analysis allows the user to capture frequency changes over time. When applied to audio processing, STFT is usually used with window lengths ranging from 10 to 120 ms that overlap by 50 or 75% [27]. Through extensive offline tuning, the optimal settings for the STFT analysis were selected as a window length of 2500 samples (approximately 98 ms) and a window overlap of 75%. Time, frequency, and time-frequency domain plots illustrated in this study were carried out using in-house developed MATLAB codes.

The flowchart depicted in Fig. 4 shows the sequential steps used to process the acoustic data acquired from the WAAM process, with the intent of characterizing the effects of contaminations on the acoustic signal.

3. Results and discussion

3.1. WAAM parts characterization

As discussed in Section 2.2, contaminants were placed on the surface of the part to induce flaw formation. Fig. 5(a) depicts the side view of the thin-wall S1, contaminated with sand. Fig. 5(b) and (c) illustrates the XCT scan and a cross section of the top layer respectively. Referring to the XCT from Fig. 5(b), small pores are observed with an irregular morphology (represented by the small blue dots) throughout the layers. Additionally, two large pores are pointed out by arrows on Fig. 5(b). The location of these larger pores is coincident with the location of sand contaminant particles (layer #11). Pertinently, the sand particles located in layer #7 were not detected in the XCT analysis. This is likely because the flaw was suppressed due to partial remelting of the layer when depositing the next one.

After confirming that the contaminant materials did generate defects on the walls produced by WAAM, the acoustic data from the components that comprise the WAAM equipment were analyzed to avoid misidentification of defects.

3.2. Sound spectrum external to the WAAM process

Prior to analysis of the signals, we isolated the noise resulting from

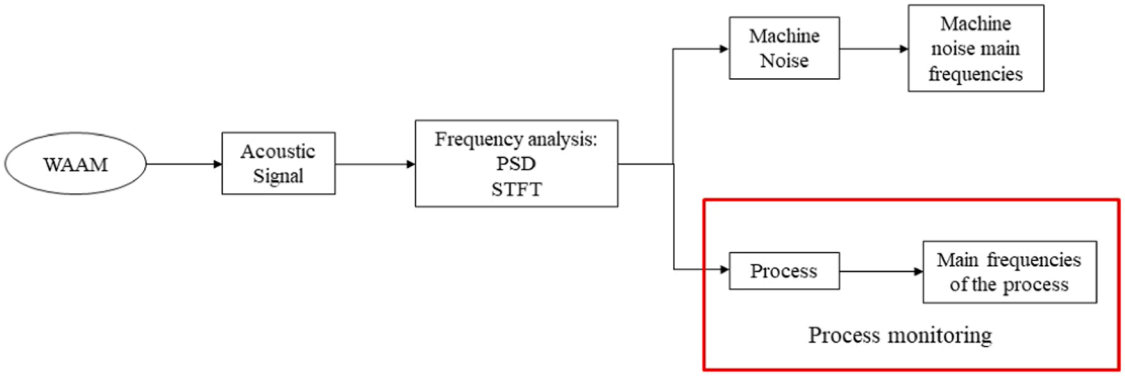

Fig. 4. Flowchart of the processing of the acoustic signal of the WAAM process.

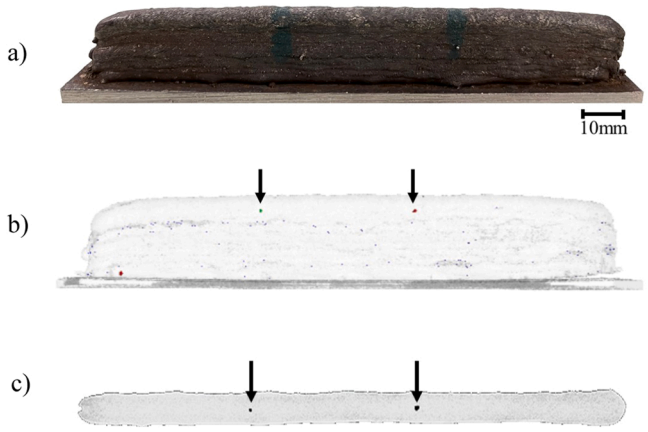

Fig. 5. Sample S1, contaminated with sand. (a) Side view of the build (b) XCT scan of the build (c) cross section of the top layer. The arrows detail the location of the defects generated. (For interpretation of the references to colour in this figure legend, the reader is referred to the web version of this article.)

the machine elements and examined the acoustic data on the time-frequency domain with the STFT algorithm, to identify the main frequencies and intensity of the associated signals. Fig. 6 depicts the STFT representation of the acoustic signal generated by the fume extraction system, shielding gas, wire extruder, and welding torch movement at a travel speed of 360 mm/min, respectively. For these time-frequency representations, the operating period of the components is marked with a dashed black box and the characteristic frequencies generated by each of the components are signaled with a red arrow in the yy axis. Table 4 summarizes the main frequency ranges identified for each of the WAAM components through time-frequency domain analysis.

The STFT plots represented in Fig. 6 show that in the absence of any functioning component there is constant background noise in the frequency range of 0–500 Hz. Due to this background noise, this frequency range was discarded from the analysis performed in this work. Although this frequency range could have been removed from the signal by using a high pass filter, the application of this filter did not improve defect identification or characterization on the time nor the frequency domains, so it was chosen to show the full frequency range captured by the microphone. In contrast with the low operating frequencies presented in Table 4, the causal phenomena of the WAAM process occurs over the frequency ranges of 3.15–4, 4.2–5, 5.8–7.3 and 7.7–9.2 kHz as it will be evidenced on Section 3.5.1. Although the frequency response of the shielding gas overlaps with the process frequency ranges, the shielding gas has a considerably lower intensity.

The power contained on each of these frequency ranges was calculated for all the equipment and for a flaw free layer using the PSD average over those ranges and plotted in Fig. 7.

From Fig. 7 it is evident that the acoustic signal generated by the machine elements presents a significantly lower intensity over the selected frequency ranges, when compared to the WAAM process showing that the acoustic signal of the external equipment has no impact on the signal that originates from the process. Thus, the effect of the WAAM equipment can be suppressed during analysis of the acoustic signal generated by WAAM (further detailed in Fig. 11). It should also be noted that a 95% confidence interval was represented for each of points plotted, however, due to the high number of samples and large scale of the yy axis in Fig. 7, the confidence interval cannot be observed.

3.3. Acoustic spectrum of the electric arc

As documented in the existing literature, the sound emitted by the WAAM process originates from two separate mechanisms [25,28]. The dominant noise in the WAAM acoustic is referred to as impulse noise and is caused by the metal droplet transfer and subsequent arc ignition (characterized by peaks of higher intensity) and arc extinction (characterized by peaks of smaller intensity). The other acoustic generating mechanism is referred to as turbulent noise and consists of low amplitude noise mainly caused by the oscillation of the electric arc and molten pool, as well as release of internal tensions.

The acoustic signature was isolated layer-by-layer for each part. Fig. 8(a) depicts the acoustic signal for the deposition performed in layer #6 from sample S1 (sand contamination). The zoomed in portion of the signal shown in Fig. 8(b) details the sound pulses from the region highlighted in green in Fig. 8(a). Fig. 8(c) depicts the respective voltage and current values, represented in black and red, respectively.

In Fig. 8(c), the large upward spikes correspond to a short circuit, i.e., a positive current peak and a voltage drop. To explain further, Fig. 9 depicts the sound spectrum for the ignition and extinction of one electric arc. Such one-to-one comparison between the acoustic and electric data enables identification of the acoustic signatures correlated to arc fluctuations. In Fig. 9 the impulse noises were identified and was seen that these are evanescent, impulse-type signatures. Between these two peaks a period of turbulent noise was also identified. After the arc extinction, only background noise is captured, with the voltage values dropping to approximately zero.

After the identification of the main frequencies of each of the components of the WAAM system and validation of the acoustic data obtained, it is now possible to analyze the sound spectrum during production of the 316L WAAM parts.

3.4. Reference signal characterization

To identify any anomaly in the acoustic data recorded we first delineate, a so-called *characteristic reference signal* that is representative of a flaw-free layer. In Fig. 10, the PSD plot for three flaw-free layers, one layer from each of the samples, is depicted highlighting the similarity of

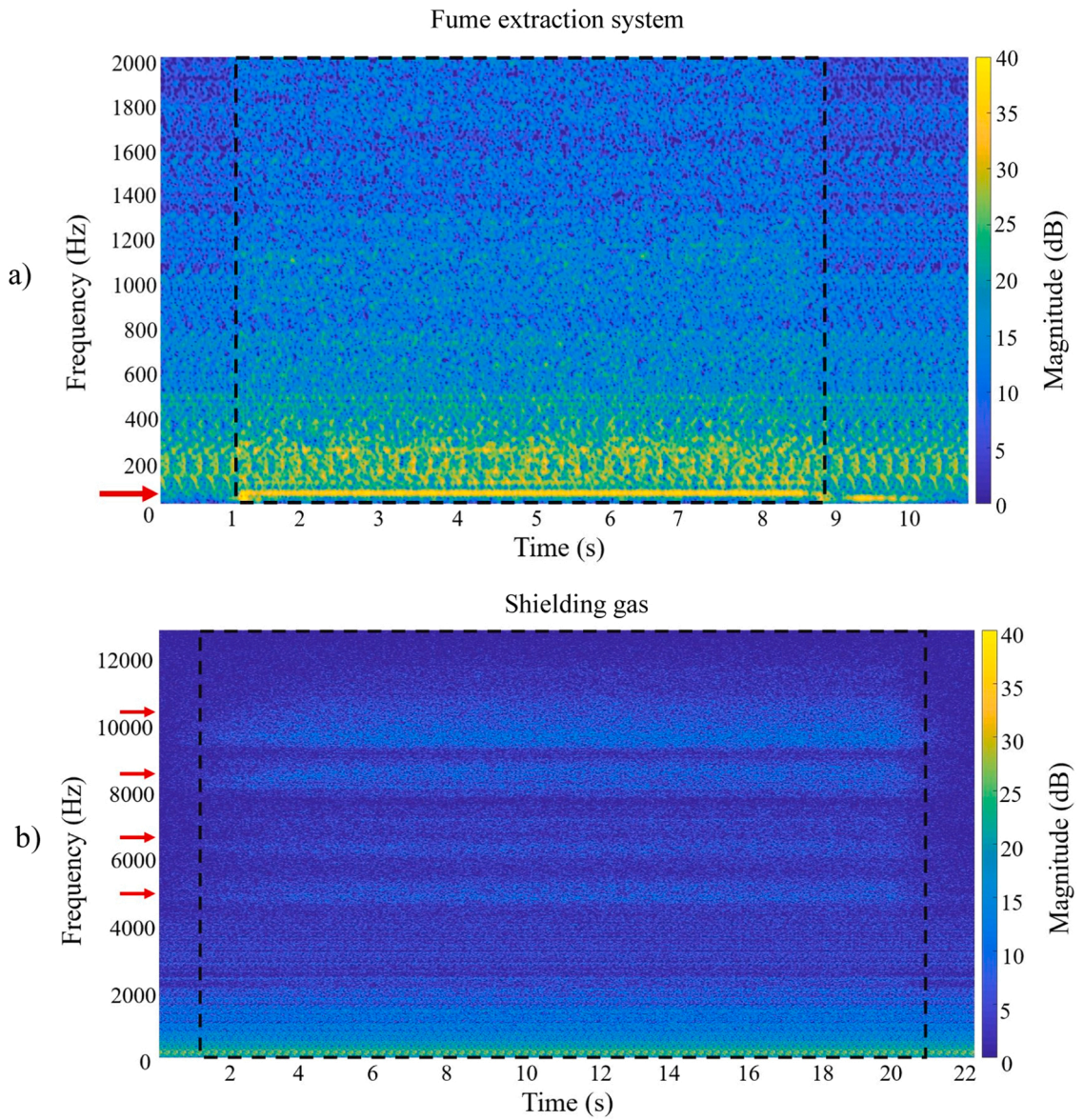

Fig. 6. STFT representation of the acoustic signal generated components that comprise the WAAM equipment. (a) Fume extraction system. (b) Shielding gas. (c) Wire extruder. (d) Welding torch movement at 360 mm/min. (For interpretation of the references to colour in this figure legend, the reader is referred to the web version of this article.)

the signal for all three different layers.

Fig. 10 shows that the deposition of flaw-free layers produced acoustic signals that were very similar to each other despite some small local variations in magnitude. This change in the frequency of the acoustic data can be attributed to the high intrinsic instability of the WAAM process when compared to other AM processes, such as those based on laser or electron beam. Since the WAAM acoustic signal displays such consistency, i.e., the same trend and very similar magnitudes for most of the frequency ranges for flaw-free layers, this allowed for the selection of one single signal (reference signal) that is representative of a flaw-free deposition.

Exemplified in Fig. 11(a) is a reference signal captured from a flaw-free layer (layer #6) of sample O1. The flaw-free nature of this layer was based of our previous knowledge on building 316L stainless steel parts by WAAM [13] and subsequently confirmed by XCT analysis and post-process materials characterization. From Fig. 11 (a), the challenges of pinpointing the effects of flaw formation on the acoustic signal are further magnified – the acoustic signal obtained from the WAAM process is complex, replete with high-frequency, short-lived sharp peaks with variable amplitude.

The STFT procedure is applied to the reference signals, the results of which are shown in Fig. 11(b); therein it is possible to identify four prominent frequency ranges, limited by the dashed black boxes, that are observed throughout the deposition process (apart from the noise from the equipment). These frequencies spectra regions are:

- 3.15–4 kHz.
- 4.2–5.5 kHz.
- 5.8–7.3 kHz.
- 7.7–9.2 kHz.

Further, on comparing Figs. 8(a), 9(a), and 11(a) from the time domain analysis, it is evident that the acoustic signature from the WAAM process has a significantly higher intensity than the equipment-related noise. The main frequencies on the reference signal are also higher than those from the equipment thus allowing separation of the process

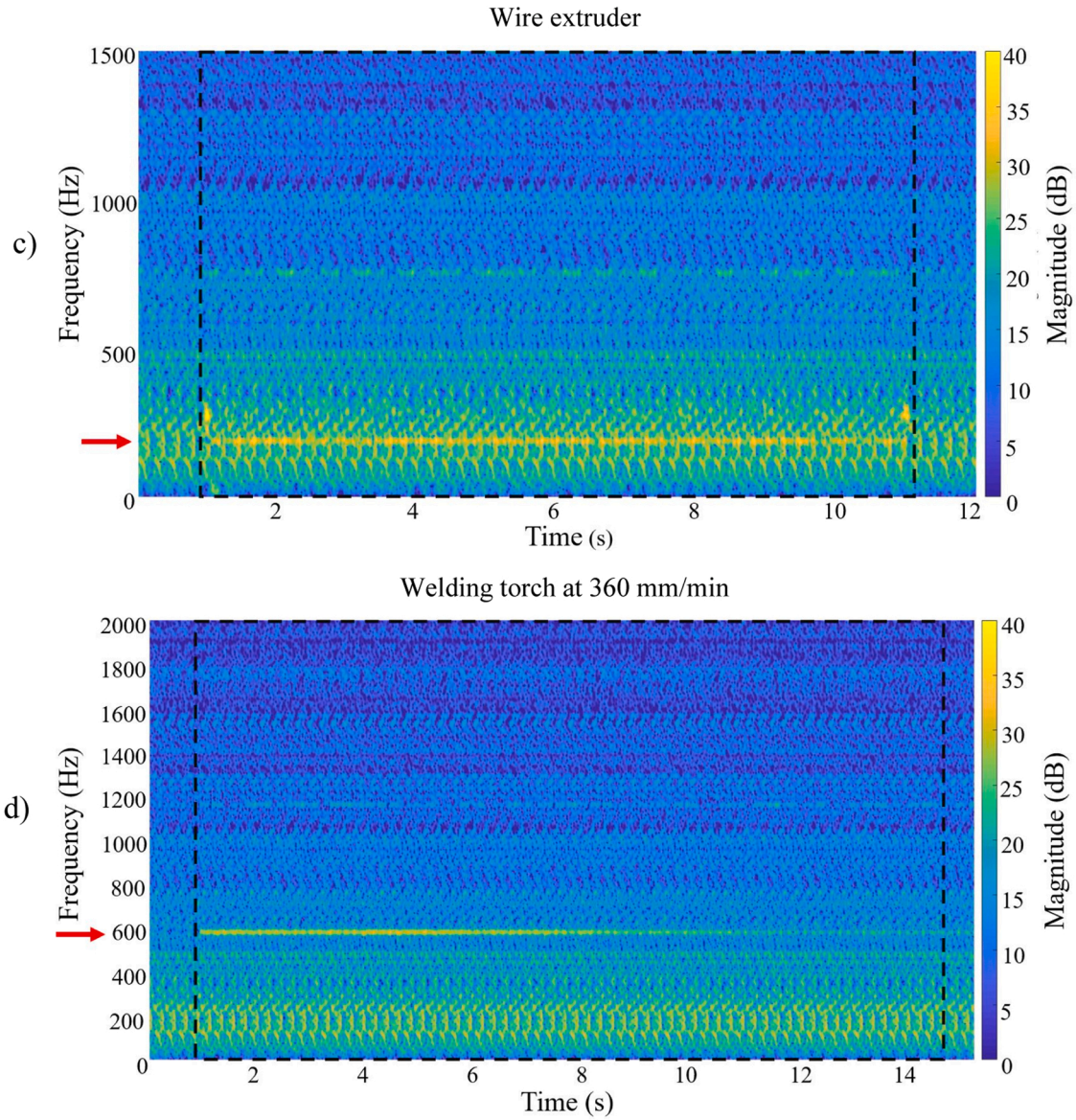

Fig. 6. (*continued*).

Table 4
Main frequency ranges identified in each component of the WAAM equipment.

Equipment	Main frequency ranges [Hz]
Fume extraction system	45–60
Shielding gas	4600–5100
	5800–7000
	8000– 8800
	9300–10,500
Wire extruder	140–290
Welding torch at 360 mm/min	560–590

signatures from extrinsic noise. Next, we define the acoustic variations caused by processing defects induced by the presence of contaminating materials.

3.5. Effects of different contaminant materials on arc stability

3.5.1. Effect of process faults induced due to chalk particle contaminants

Fig. 12(a) and (b) depicts the time domain and STFT plots for the acoustic signal from layer #7 of sample C1, upon which chalk was added to aid in arc disruption aiming to create defects. Since the chalk particles are a poor conductor of electricity, their presence on the part surface creates a momentary instability in the electric arc. The few seconds where the electrical arc cannot be established between the electrode and already deposited material are liable to cause flaw formation, such as lack-of-fusion and/or porosity that will ultimately affect the mechanical performance of the as-built part. In the time series plot show in Fig. 12 (a), the regions highlighted in green are affected by the presence of chalk particles. In this time series plot, a low amplitude region manifests in the region of contamination due to arc instability. Fig. 13 depicts a zoomed in portion of the first region highlighted in green (also on time domain). This representation shows that the presence of the chalk particles resulted in low amplitude turbulent noise followed by intervals where only background noise was captured. Similarly, the STFT plot in Fig. 12 (b), shows that the region with contamination is characterized by low intensity intervals interspersed with short sound peaks.

Even though the existence of a contaminant that promotes arc disruption is obvious through the time domain and STFT analysis, to understand the nature of change in the frequency components due to the presence of chalk particles, we calculated the PSD of the acoustic signal. Fig. 14 depicts the PSD plots of the contaminated layers (#7 and #11),

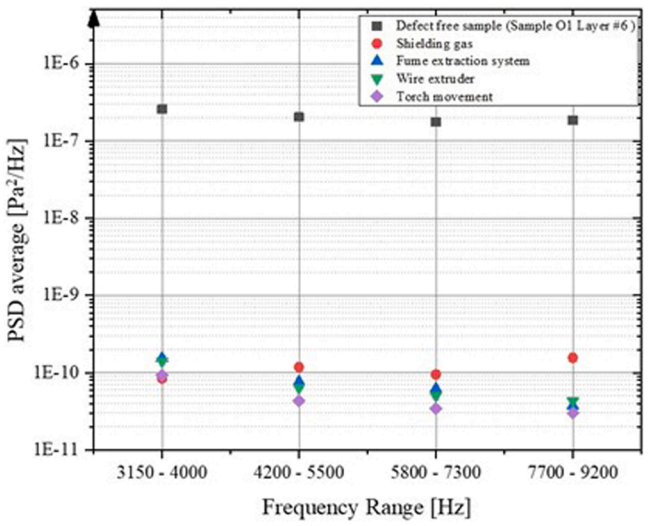

Fig. 7. Power spectral density (PSD) average over the main frequency ranges of the acoustic signal of the WAAM process.

and of the reference layer (#6). All the PSD plots analyzed in this study generated variable results, even for layers printed on similar conditions, so only the main frequencies of each contaminated zone will be further characterized and discussed.

The PSD plots show variations on both signals from contaminated layers (black and red curves in Fig. 14) when compared to the reference signal (green curve in Fig. 14). However, the frequency components of the acoustic signals for the contaminated layers do not exhibit variations in agreement with each other, so, from the PSD of the full depositions, it was not possible to identify a range of frequencies that were altered by the presence of the contaminating material and subsequent arc disruption. This lack of significant variation in frequency shows that the effect of the contaminant material on the acoustic data was not enough for this to be noticeable when the whole deposition is considered.

To avoid the attenuation of the contaminated region due to the length of the signal, the PSD algorithm was applied to a 1 s interval in the contaminated area, as illustrated in Fig. 15. The reference signal illustrated in Fig. 15 was defined from a 1 s interval of the reference layer defined for this study (refer to Fig. 11). This time range was selected considering the smallest time interval on which the chalk affected the deposition process. To further demonstrate the repeatability of results, contaminated regions from different layers were also considered.

The data for both contaminated layers present a lower intensity than the reference for most of the frequencies analyzed since the regions affected by the chalk particles resulted in a low intensity acoustic signal, as previously stated. In addition to the difference in signal intensity, frequency variations that are consistent for the contaminated signals were also identified (black regions in Fig. 15). The differences between a reference layer and layers with chalk are quite pronounced in the frequency ranges of [3.1; 4], [4.5; 5.3], [5.8; 7.1], and [8; 9.2] kHz, as detailed in Fig. 15. These differences in frequency were verified for the four chalk contaminated areas introduced in this sample.

The results obtained from the layers contaminated with chalk lead to the conclusion that the presence of chalk during a layer deposition with the WAAM process is identifiable on time domain and through the STFT representation. These representations, however, do not allow for the frequency characterization induced by the preplaced contamination. To define these frequency variations, the application of the PSD to a 1 s interval proved to be a successful method. To verify how the changes caused by the preplaced contaminants are affected by the selection of the time interval (1 s vs full signal) used on the PSD analysis, the characterization of frequency alterations triggered by the presence of oil and sand was carried out using the same procedure used for the characterization of the defects that result from the chalk contamination.

3.5.2. *Effect of process faults induced due to oil contaminants*

Similarly to what was observed for the chalk contamination, the oil contamination will also affect the stability of the electric arc even though in a less impactful way. Due to the high temperatures, the

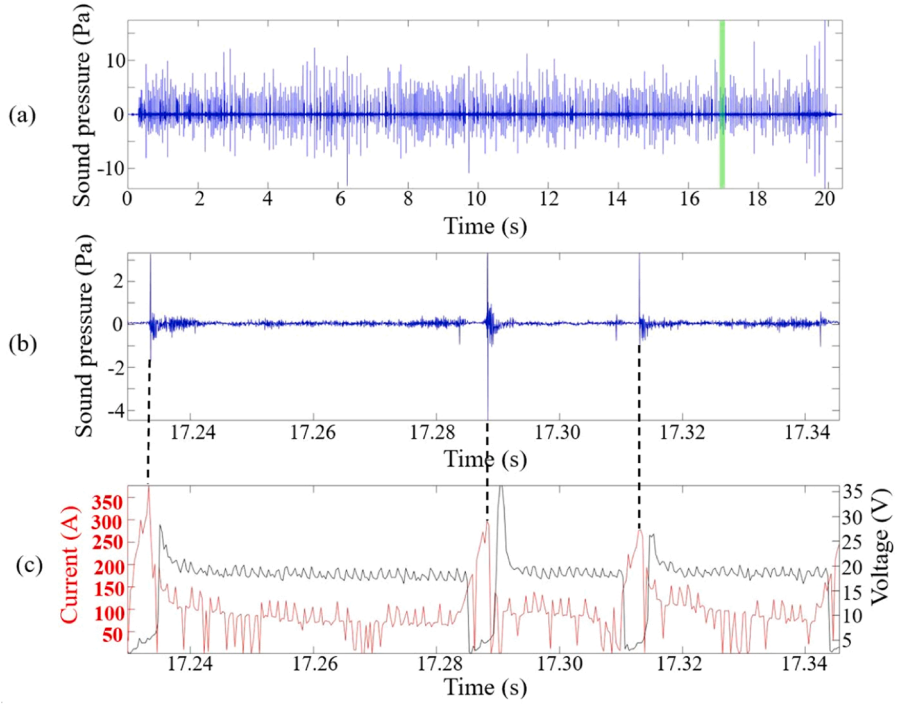

Fig. 8. (a) Acoustic signal generated by the deposition of layer #6 from sample S1. (b) Acoustic signal of the zone highlighted in green (c) Correspondent electrical current and voltage signals. (For interpretation of the references to colour in this figure legend, the reader is referred to the web version of this article.)

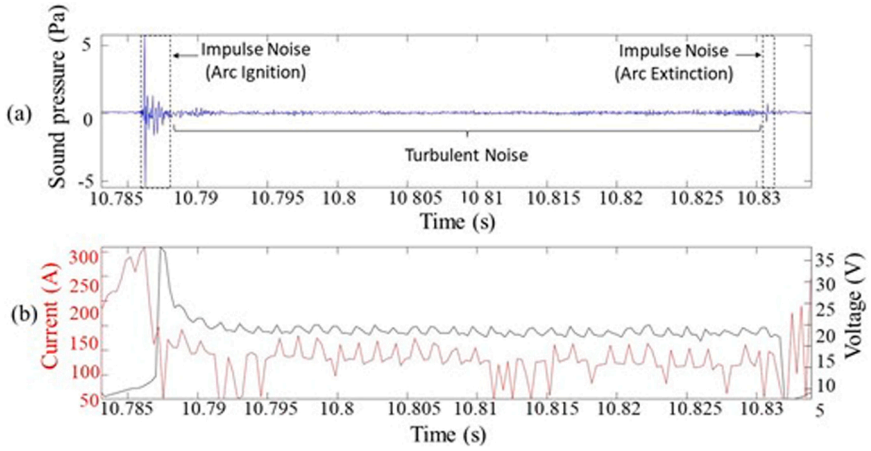

Fig. 9. Acoustic signal generated by one electric arc. (b) Corresponding electrical current and voltage signals.

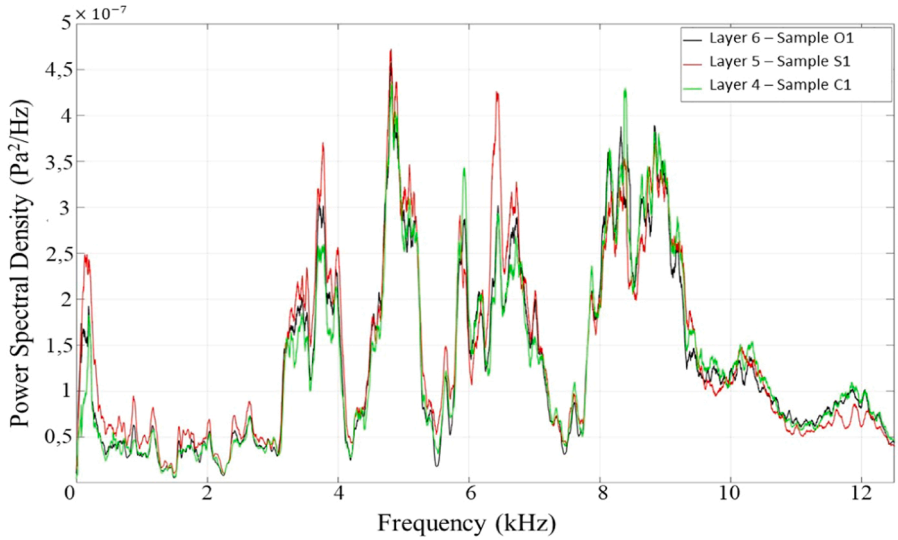

Fig. 10. PSD plot for three flaw free layers.

hydrogen from the evaporation of the oil will be absorbed by the molten pool thus resulting in porosity. Fig. 16 depicts the acoustic signal for layer #11 of sample O1. On both time and time-frequency representations, the areas where the contamination occurred were highlighted.

As evident from Fig. 16, the presence of oil is not as perceptible on the time domain as it was for chalk since oil does not fully inhibit the formation of the electric arc during WAAM. Since the STFT representation in the contaminated areas does not show mutually concordant frequency variations that can be attributed to the presence of oil on the deposited layer, it is necessary to apply the PSD algorithm as detailed in Fig. 17, in which the signals for the complete deposition of layers #7 and #11 from sample O1 and the reference layer (#6) were represented.

The PSD analysis of the full deposition of the oil contaminated layers shows clear differences between the reference layer and the contaminated layers. The frequency ranges [2.2;3.5], [4.1;4.4] and [7.2;7.8] kHz show peaks of higher intensity for the contaminated layers while the reference signal displays a much lower intensity for the same ranges. The frequency range [5.1;5.7] kHz shows a clear drop in intensity for all the signals represented, however the minimum for this interval is located at 5.3 kHz for the contaminated signals while for the reference signal it is at 5.5 kHz. Although some variations can also be identified above 9.2 kHz, these were not considered as indicative of a defect because these are outside of the frequency spectra regions previously defined for the WAAM process (refer to Fig. 11).

Similarly to what was applied for the chalk particles contamination, the PSD was applied to a 1 s interval inside of the contaminated areas (refer to Fig. 18). From this analysis it is observed that the frequency ranges [7.3;7.8] and [8.5;9.2] kHz have a higher intensity than the reference signal while the intervals [4.7;5.2] and [6.1;6.5] and kHz are below the reference. This highlights the ability of such procedure to indicate potential regions where non-stable processing conditions, in this case induced by introduction of a contaminant material, during WAAM may occur.

Since the PSD represented on Fig. 18 only considers the contaminated region (for layers #7 and #11) this leads to the conclusion that the frequency ranges highlighted on the figure can be indicative of a potential arc instability induced by the presence of oil at those predefined locations. The application of the PSD to the contaminated zones shows that it is possible to identify the changes in the acoustic spectrum caused by the presence of oil on the deposited layers using both 1 s interval and full signal analysis. However, this feature becomes more evident when the 1 s analysis is applied.

On both PSD plots for the deposition of layer #7 it can be noted that the frequency range of [0; 0.24] kHz shows a significantly higher intensity than the other signals represented. However, as mentioned earlier, this frequency range was not considered due to the constant background noise that was captured. Further studies are planned to address the analysis of this low frequency region.

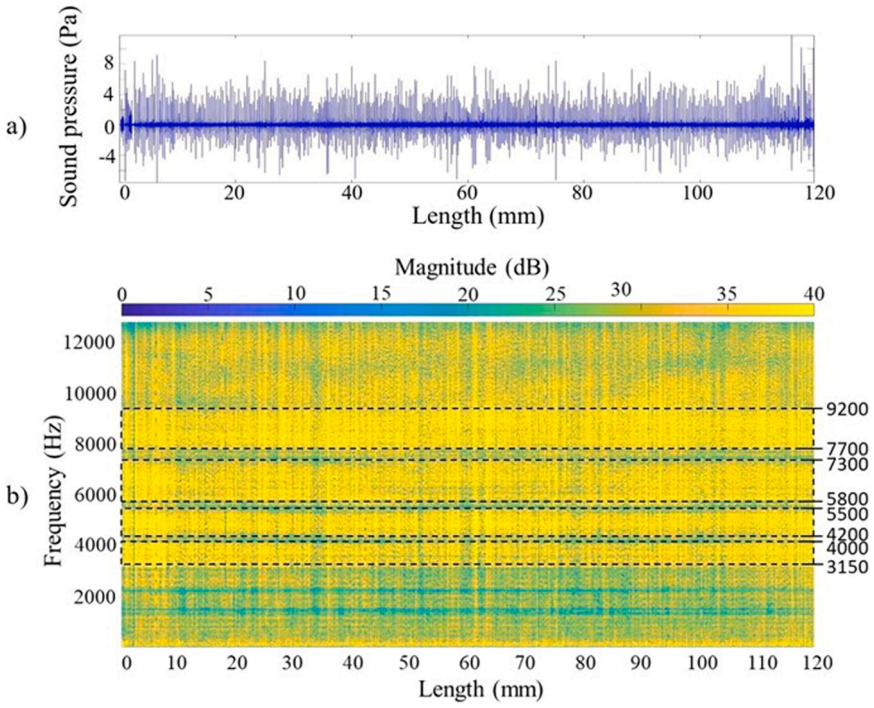

Fig. 11. Acoustic signal from layer 6 of sample O1. (a) Time domain representation. (b) Time- frequency domain representation.

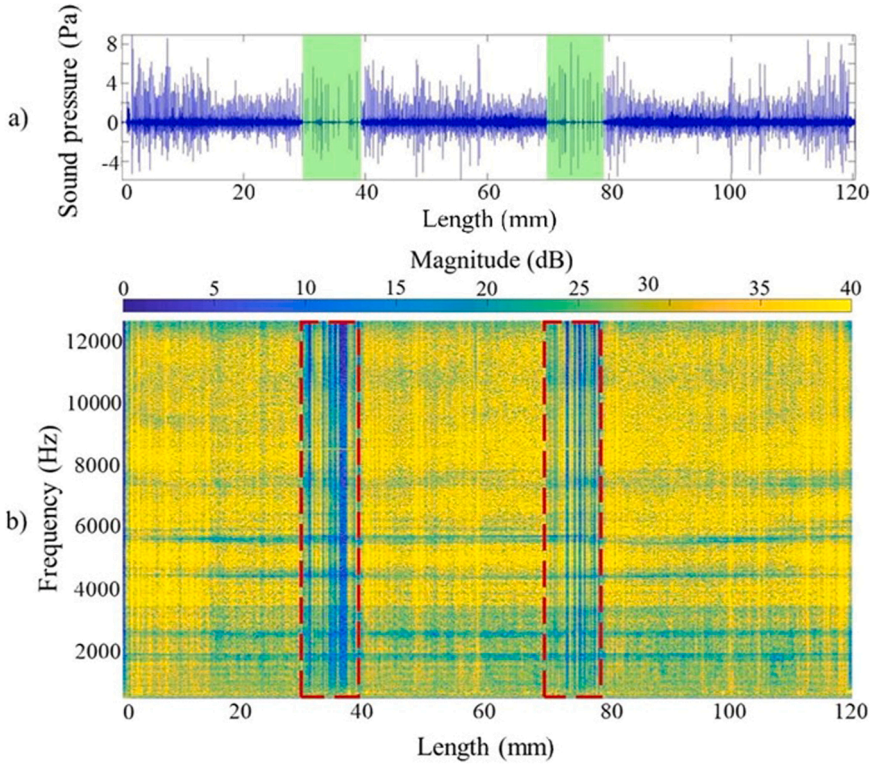

Fig. 12. Acoustic signal obtained during deposition of layer #7 of sample C1. a) Time domain representation. b) Time- frequency domain representation. The green regions in a) indicate where perturbation of the sound pressures occurs, which correspond to the areas outlined by the red boxes. (For interpretation of the references to colour in this figure legend, the reader is referred to the web version of this article.)

3.5.3. Effect of process faults induced due to sand particle contaminants

Sand, just like chalk, is a very poor electrical conductor and is expected to disturb the electric arc. Comparatively to chalk, sand has a lower compaction ratio which can result in partial particle removal from the shielding gas, thus reducing the impact of the contamination on the deposited layer. The acoustic signal for the deposition of layer #7 from sample S1 is illustrated on Fig. 19, with the contaminated zones highlighted on both time and time-frequency domains. Despite not being able to identify the presence of sand through the time domain analysis on Fig. 19a), the effect of this contaminant material is visible through

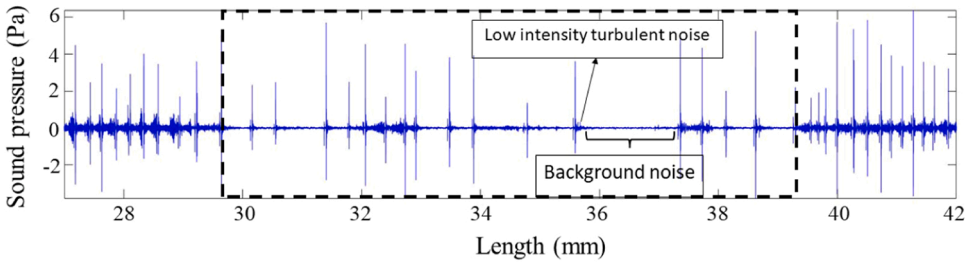

Fig. 13. Time domain representation of the first chalk-contaminated area of layer #7 from sample C1.

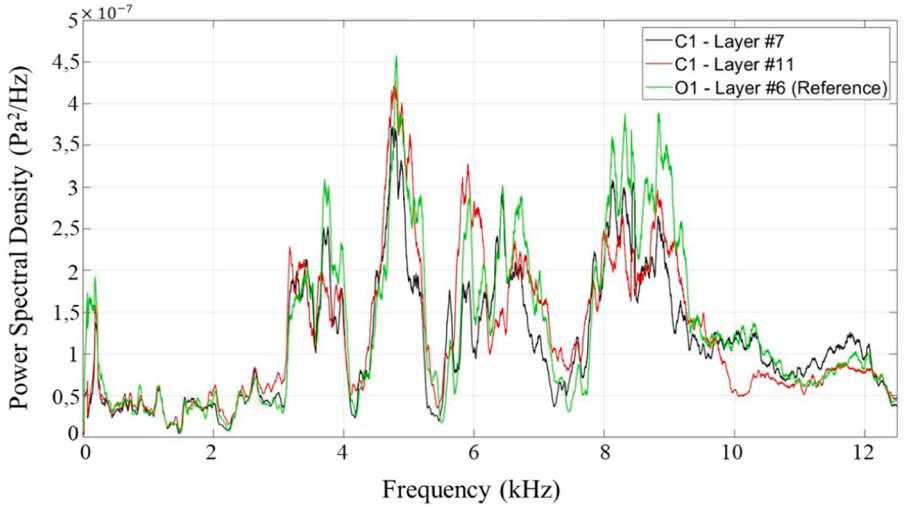

Fig. 14. PSD plots for the deposition of the contaminated layers (#7 and #11) from sample C1 and reference (defect-free) layer #6 from sample C1, used as reference. (For interpretation of the references to colour in this figure legend, the reader is referred to the web version of this article.)

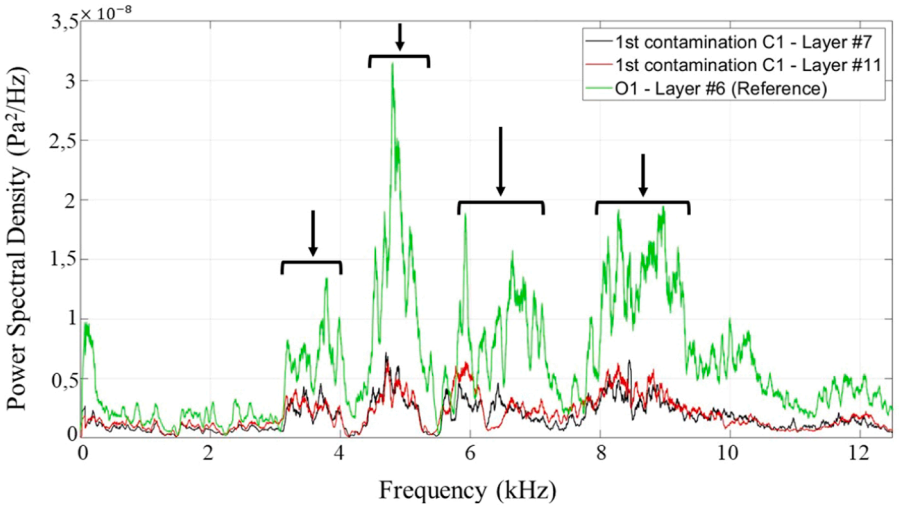

Fig. 15. Power Spectral Density (PSD) plot for a 1 s interval inside the contaminated layers #7 and #11 from sample C1 and layer 6 from sample C1, taken as reference. The black arrows indicate the frequencies that differ greatly from the reference signal.

the STFT representation depicted in Fig. 19b).

From the analysis of the time-frequency domain representation a sudden drop of intensity can be noted on the frequency range of [7.09;7.35] kHz, so it is expectable that this is one of the frequency ranges that will allow the identification of the effect of sand on the WAAM process. Time-frequency domain analysis from Fig. 19b) also showed the existence of variations, that have no known cause, for frequencies above 8.9 kHz. These apparently random signal changes only occurred in sample S1.

To make a more precise identification of how the sand is altering the frequency of the acoustic signal, the PSD was applied, as illustrated in Fig. 20, to the entire deposition of layers #7 and #11, contaminated with sand.

As was observed for the signals plotted in Fig. 17, the frequency range [2.2;3.5] kHz has a higher intensity for the contaminated signals. However, there is a large variation between the signals with

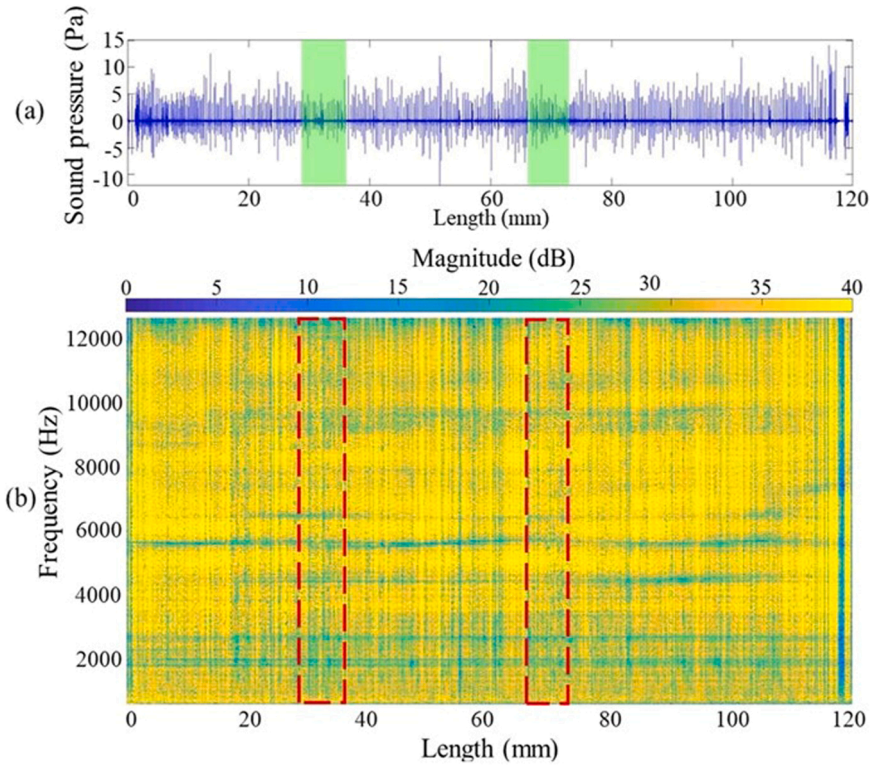

Fig. 16. Acoustic signal from layer #11 of sample O1. a) Time domain representation. b) Time- frequency domain representation.

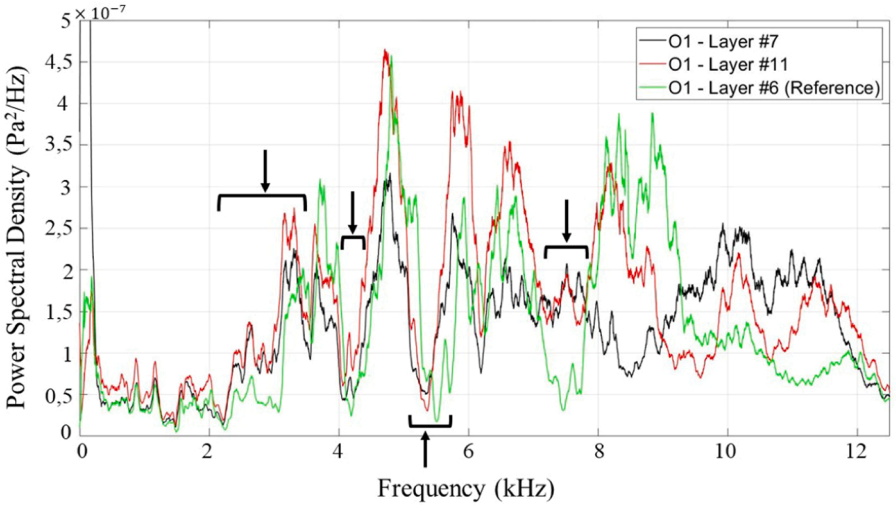

Fig. 17. Power Spectral Density (PSD) plots for the deposition of the contaminated layers #7 and #11 from sample O1 and layer #6 from sample C1, used as reference.

contaminants. Due to this clear discrepancy between the contaminated signals, the 1 s PSD analysis (inside the sand contaminated region), illustrated in Fig. 21, was applied.

On the 1 s interval analysis it was noticed that the frequency intervals [5.4; 5.7], [7; 7.5] and [8.2; 8.6] kHz have a lower intensity than the reference. No significant variations on these frequency ranges were perceptible on the PSD analysis for the full deposition of the contaminated layer, which indicates that for the identification of this potential process disruption it is necessary to analyze the 1 s interval PSD plot. The frequency ranges identified on the full signal analysis (refer to Fig. 20) are not observed on the 1 s interval PSD analysis which indicates that they are not related to the presence of sand on the layer.

The analysis of the set of data collected from each of the samples, allow us to conclude that contaminations in the WAAM process can be characterized through the analysis of the acoustic spectrum of the process. By using different contaminant materials, which in turn have distinct effect on the arc disruption and stability, it was possible to clearly identify the regions where these process instabilities occurred. Through the analysis of the frequency components of the signals it is possible to characterize the effect that the pre-placed contaminations have on the acoustic signal. The consistency of the frequency variations also show that different contaminant materials result in the alteration of distinct frequency ranges allowing their differentiation. The application of the PSD to an interval of 1 s inside the contaminated areas was the method that displayed the greatest difference between contaminated regions and the reference signal. As it was previously demonstrated on

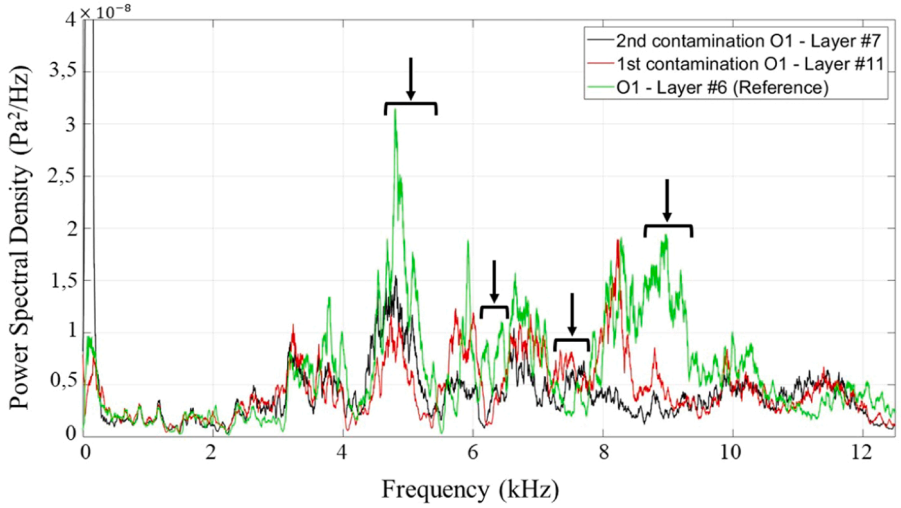

Fig. 18. Power Spectral Density (PSD) plots for a 1 s interval inside the contaminated layers #7 and #11 from sample C1 and layer #6 from sample O1, taken as reference.

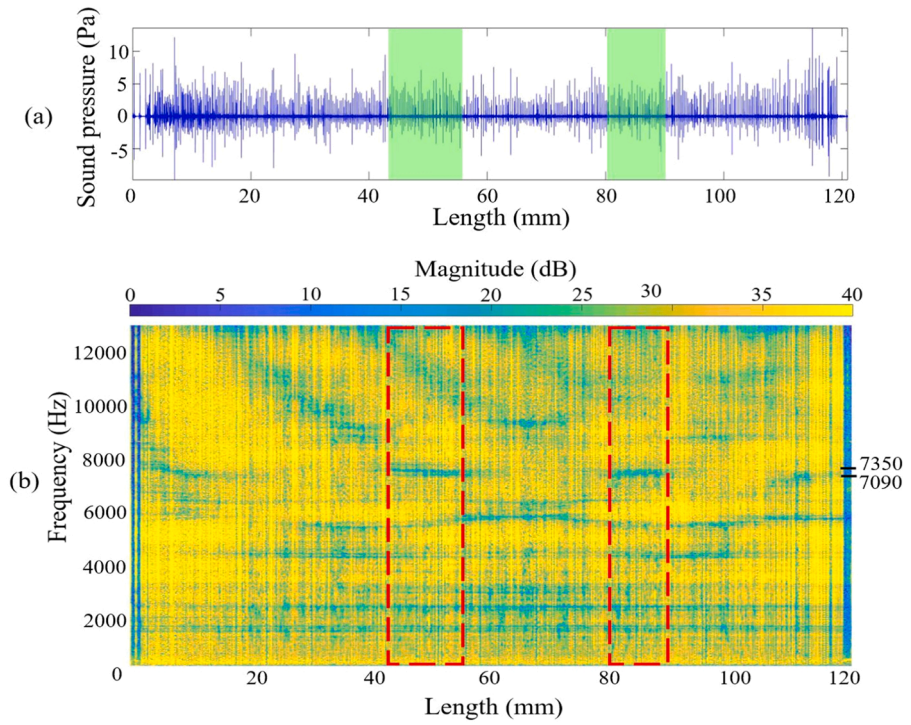

Fig. 19. Acoustic signal from layer #7 of sample S1. a) Time domain representation. b) Time-frequency domain representation.

the time and time-frequency representations of the acoustic data, refer to Fig. 12a) and b) respectively, the use of the STFT and the graphical representation of the sound pressure allow to determine the location of the potential defects (in this case induced by pre-placed contaminants) along the deposited layers. Future and ongoing work will focus on detection of defects through the application of machine learning algorithms, either through supervised and/or unsupervised learning, to aid in the implementation of acoustic monitoring for the WAAM process.

4. Conclusions

This study aimed to evaluate the effects of contaminant materials on the acoustic spectrum of the WAAM process based on the analysis of the corresponding time and frequency domains. The identification and location of process disruptions, promoted by the insertion of contaminant materials at predefined positions within the fabricated WAAM walls, was evidenced. The following major conclusions can be drawn:

The existence of a constant noise in the frequency range of 0–500 Hz limits the available frequency range of analysis, making it only viable to clearly evaluate the 500–12,600 Hz interval.

The characterization of the acoustic spectrum of the functioning components showed that these produce low intensity sounds and low frequencies when compared to the WAAM process, and therefore can be suppressed during analysis since they have no significant effect on the acoustic spectrum generated by the deposition process.

A reference signal was defined considering a flaw free layer (confirmed by XCT analysis and post-process materials characterization). The STFT analysis of this reference signal allowed for the

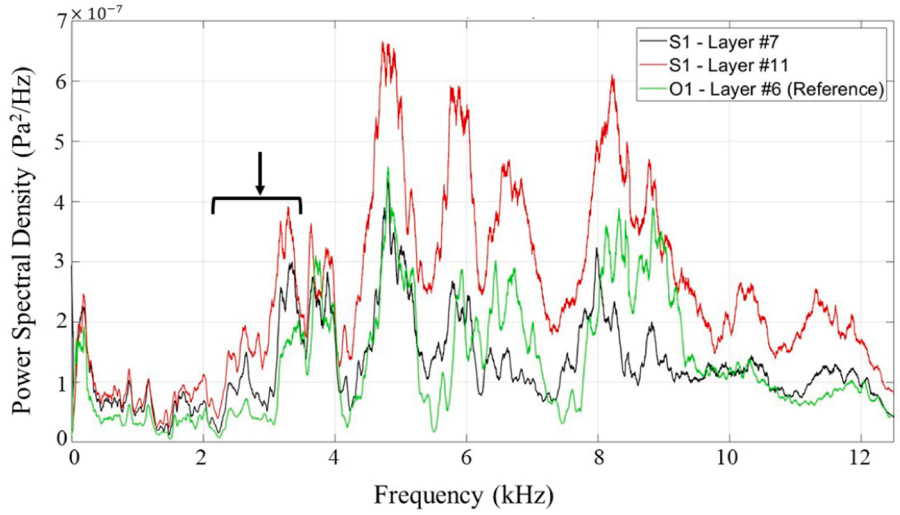

Fig. 20. Power Spectral Density (PSD) plots for the deposition of the contaminated layers #7 and #11 from sample S1 and layer 6 from sample C1, taken as reference.

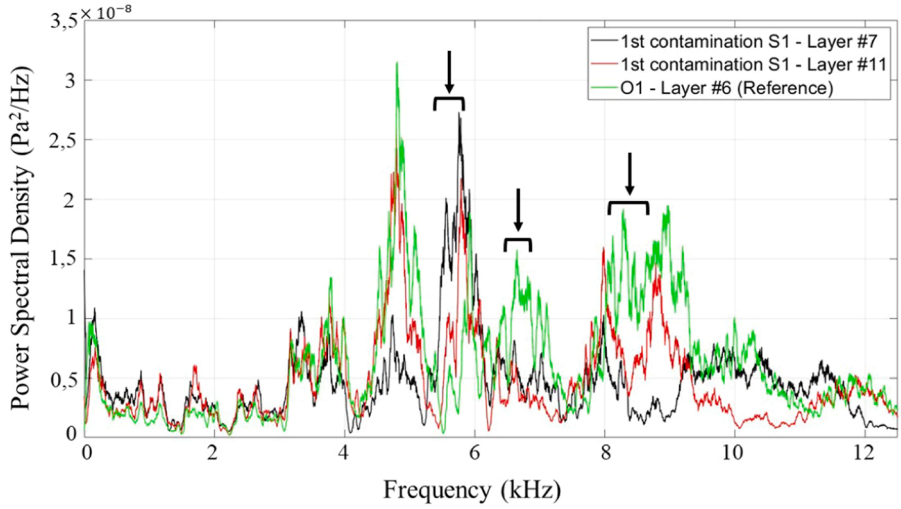

Fig. 21. Power Spectral Density (PSD) plot for a 1 s interval inside the contaminated layers #7 and #11 from sample S1 and layer #6 from sample C1, taken as reference.

identification of four frequency ranges with high intensity and small variation over time.

The data collected for the deposition of the contaminated layers showed that the location and identification of the process instabilities is possible through the analysis of the acoustic spectrum. Time domain and time-frequency domain analysis allowed for the spatial location of the disruption of the electric arc induced by the presence of contaminants. Even though the STFT plot shows the frequency variations over time, the subtle frequency variations caused by the preplaced contaminants are hard to characterize using this method.

The PSD plot of the contaminated layers allowed for the identification of different frequency variations for each of the contaminants used in this study. The characterization of the effect of the contaminant materials was carried out by applying the PSD analysis to both full deposition and 1 s interval in the contaminated region. The identification of these potential defective regions became more evident when applying the PSD at the 1 s interval, enabling the identification of subtle variations, indicating that this should be the method to apply when analyzing the acoustic spectrum of the process.

The ability to differentiate a flaw free layer from a flawed layer by using the methods of acoustic data analysis considered in this study, paves the way for an expedite online monitoring methodology.

Although it was possible to identify the signal variations with the methods used, these show many variations even for layers deposited under identical conditions. This indicates that other methods of digital signal analysis that allow for a more effective analysis of a signal composed of sharp peaks, can and should be applied.

Future and ongoing work will focus on the detection of defects through the application of machine learning algorithms, either through supervised and/or unsupervised learning, to aid in the implementation of acoustic monitoring for the WAAM process.

CRediT authorship contribution statement

André Ramalho: Investigation, Writing – original draft, Formal analysis. **Telmo G. Santos:** Investigation, Methodology, Supervision, Formal analysis, Writing – review & editing. **Ben Bevans:** Investigation. **Ziyad Smoqi:** Investigation. **Prahalad Rao:** Investigation, Writing - review & editing. **J.P. Oliveira:** Conceptualization, Investigation, Methodology, Formal analysis, Supervision, Writing – review & editing.

Declaration of Competing Interest

The authors declare that they have no known competing financial interests or personal relationships that could have appeared to influence the work reported in this paper.

Acknowledgements

AR acknowledges Fundação para a Ciência e a Tecnologia (FCT-MCTES) for funding the Ph.D. Grant UI/BD/151018/2021. AR, TGS and JPO acknowledge Fundação para a Ciência e a Tecnologia (FCT-MCTES) for its financial support via the project UID/00667/2020 (UNIDEMI). PR acknowledges funding from the Department of Energy (DOE), Office of Science, under Grant number DE-SC0021136, and the National Science Foundation (NSF) [Grant numbers CMMI-1719388, CMMI-1920245, CMMI-1739696, CMMI-1752069, PFI-TT 2044710, ECCS 2020246] for funding his research program. This work espousing the concept of online process monitoring in WAAM was funded through the foregoing DOE Grant (Program Officer: Timothy Fitzsimmons), which supported the doctoral graduate work of Mr. Benjamin Bevans.

References

[1] C. Li, Z.Y. Liu, X.Y. Fang, Y.B. Guo, Residual stress in metal additive manufacturing, Procedia CIRP 71 (2018) 348–353, https://doi.org/10.1016/j.procir.2018.05.039.
[2] Y. Zhang, L. Wu, X. Guo, S. Kane, Y. Deng, Y.-G. Jung, J.-H. Lee, J. Zhang, Additive manufacturing of metallic materials: a review, J. Mater. Eng. Perform. 27 (2018) 1–13, https://doi.org/10.1007/s11665-017-2747-y.
[3] G. Piscopo, E. Atzeni, A. Salmi, A hybrid modeling of the physics-driven evolution of material addition and track generation in laser powder directed energy deposition, Materials 12 (2019) 2819, https://doi.org/10.3390/ma12172819.
[4] A. Khorasani, I. Gibson, J.K. Veetil, A.H. Ghasemi, A review of technological improvements in laser-based powder bed fusion of metal printers, Int. J. Adv. Manuf. Technol. 108 (2020) 191–209, https://doi.org/10.1007/s00170-020-05361-3.
[5] T.A. Rodrigues, V. Duarte, R.M. Miranda, T.G. Santos, J.P. Oliveira, Current status and perspectives on Wire and Arc Additive Manufacturing (WAAM), Materials 12 (2019) 1121, https://doi.org/10.3390/ma12071121.
[6] J.P. Oliveira, T.G. Santos, R.M. Miranda, Revisiting fundamental welding concepts to improve additive manufacturing: from theory to practice, Prog. Mater. Sci. 107 (2019), 100590, https://doi.org/10.1016/j.pmatsci.2019.100590.
[7] N. Knezovi, A. Topic, Wire and Arc Additive Manufacturing (WAAM) – A New Advance in Manufacturing, Springer International Publishing, 2018, https://doi.org/10.1007/978-3-319-90893-9.
[8] N.A. Rosli, M.R. Alkahari, M.F. bin Abdollah, S. Maidin, F.R. Ramli, S.G. Herawan, Review on effect of heat input for wire arc additive manufacturing process, J. Mater. Res. Technol. 11 (2021) 2127–2145, https://doi.org/10.1016/j.jmrt.2021.02.002.
[9] F. Martina, S. Williams, Wire+arc Additive Manufacturing Vs. Traditional Machining from Solid: A Cost Comparison: A Cost Comparison, 2015, 27.
[10] V.R. Duarte, T.A. Rodrigues, N. Schell, T.G. Santos, J.P. Oliveira, R.M. Miranda, Wire and arc additive manufacturing of high-strength low-alloy steel: microstructure and mechanical properties, Adv. Eng. Mater. 121 (2021), 2001036, https://doi.org/10.1002/adem.202001036.
[11] T.A. Rodrigues, V. Duarte, J.A. Avila, T.G. Santos, R. Miranda, J.P. Oliveira, Wire and arc additive manufacturing of HSLA steel: effect of thermal cycles on microstructure and mechanical properties, Addit. Manuf. 27 (2019) 440–450, https://doi.org/10.1016/j.addma.2019.03.029.
[12] V.T. Le, D.S. Mai, T.K. Doan, H. Paris, Wire and arc additive manufacturing of 308L stainless steel components: optimization of processing parameters and material properties, Eng. Sci. Technol. Int. J. 24 (2021) 1015–1026, https://doi.org/10.1016/j.jestch.2021.01.009.
[13] V.R. Duarte, T.A. Rodrigues, N. Schell, R.M. Miranda, J.P. Oliveira, T.G. Santos, Hot forging wire and arc additive manufacturing (HF-WAAM), Addit. Manuf. 35 (2020), 101193, https://doi.org/10.1016/j.addma.2020.101193.
[14] T.A. Rodrigues, V.R. Duarte, R.M. Miranda, T.G. Santos, J.P. Oliveira, Ultracold-wire and arc additive manufacturing (UC-WAAM), J. Mater. Process. Technol 296 (2021), 117196, https://doi.org/10.1016/j.jmatprotec.2021.117196.
[15] T.A. Rodrigues, V.R. Duarte, D. Tomás, J.A. Avila, J.D. Escobar, E. Rossinyol, N. Schell, T.G. Santos, J.P. Oliveira, In-situ strengthening of a high strength low alloy steel during Wire and Arc Additive Manufacturing (WAAM), Addit. Manuf. 34 (2020), 101200, https://doi.org/10.1016/j.addma.2020.101200.
[16] W. Chen, Y. Chen, T. Zhang, T. Wen, Z. Yin, X. Feng, Effect of ultrasonic vibration and interpass temperature on microstructure and mechanical properties of Cu-8Al-2Ni-2Fe-2Mn alloy fabricated by wire arc additive manufacturing, Metals 10 (2020) 215, https://doi.org/10.3390/met10020215.
[17] A.B. Lopez, J. Santos, J.P. Sousa, T.G. Santos, L. Quintino, Phased array ultrasonic inspection of metal additive manufacturing parts, J. Nondestruct. Eval. 38 (2019) 62, https://doi.org/10.1007/s10921-019-0600-y.
[18] J.B. Bento, A. Lopez, I. Pires, L. Quintino, T.G. Santos, Non-destructive testing for wire + arc, Addit. Manuf. Alum. Parts Addit. Manuf. 29 (2019), 100782, https://doi.org/10.1016/j.addma.2019.100782.
[19] D. Saini, S. Floyd, An Investigation of Gas Metal Arc Welding Sound Signature for On-Line Quality Control High-speed Signal Data Acquisition and Computer-aided Analysis of Sound Signature May Reveal Conditions That Generate Weld Defects, 1998, pp. 172–179.
[20] F.G. Cunha, T.G. Santos, J. Xavier, In situ monitoring of additive manufacturing using digital image correlation: a review, Materials 14 (2021) 1511, https://doi.org/10.3390/ma14061511.
[21] B. Wu, Z. Pan, D. Ding, D. Cuiuri, H. Li, J. Xu, J. Norrish, A review of the wire arc additive manufacturing of metals: properties, defects and quality improvement, J. Manuf. Process. 35 (2018) 127–139, https://doi.org/10.1016/j.jmapro.2018.08.001.
[22] K. Pal, S. Bhattacharya, S.K. Pal, Investigation on arc sound and metal transfer modes for on-line monitoring in pulsed gas metal arc welding, J. Mater. Process. Technol. 210 (2010) 1397–1410, https://doi.org/10.1016/j.jmatprotec.2010.03.029.
[23] B. Chen, J. Wang, S. Chen, A study on application of multi-sensor information fusion in pulsed GTAW, Ind. Robot Int. J. 37 (2010) 168–176, https://doi.org/10.1108/01439911011018948.
[24] A. Sumesh, K. Rameshkumar, K. Mohandas, R.S. Babu, Use of machine learning algorithms for weld quality monitoring using acoustic signature, Procedia Comput. Sci. 50 (2015) 316–322, https://doi.org/10.1016/j.procs.2015.04.042.
[25] J. Horvat, J. Prezelj, I. Polajnar, M. Čudina, Monitoring gas metal arc welding process by using audible sound signal, Stroj. Vestn. – J. Mech. Eng. 2011 (2011) 267–278, https://doi.org/10.5545/sv-jme.2010.181.
[26] S.W. Smith, The scientist and engineer's guide to digital signal processing, IEEE Signal Process. Mag. 13 (2000) 141–255, https://doi.org/10.1109/79.826412.
[27] T. Virtanen, E. Vincent, S. Gannot, T. Virtanen, E. Vincent, S. Gannot, T. Spectral, E. Vincent, T. Virtanen, S. Gannot, Time-frequency Processing – Spectral Properties, 2018.
[28] K. Samvatsar, R. Barot, H. Beravala, V. Chhillar, Feasibility study for in-process monitoring of gas tungsten arc welding, Int. J. Eng. Res. Dev. 11 (2015), 2278–67.